Uncertainty-Aware Robust Dynamic Operating Envelope for Safe Integration of Distributed Energy Resources

Feixiang Zhang, Hongyi Li, *Member, IEEE*, and Zhaoyu Wang, *Fellow, IEEE*

***Abstract*—The increasing penetration of distributed energy resources (DERs) motivates the research on dynamic operating envelopes (DOEs), which are the power limits issued by utilities to DERs to ensure operational constraint compliance. However, the inherent load uncertainty and the non-convexity of power flow pose significant challenges to the optimization of DOEs. In this paper, a two-stage DOE optimization framework is proposed, where the first stage problem characterizes the optimal DOEs and the second stage problem checks the feasibility of DOE internal operating points against all possible uncertainty realizations. To ease computational burdens, a data-driven approach is leveraged to convexify the distribution power flow model for feasibility check. In this way, an efficient solution algorithm is proposed based on Benders decomposition, which converts the two-stage DOE optimization problem into two mixed-integer linear programming problems to be solved iteratively. Finally, through detailed case studies on the IEEE 123-node test feeder, the proposed method can achieve more robust and accurate DOEs than the benchmarks.**

***Index Terms*—Distributed energy resource, distribution system, dynamic operating envelope, input convex neural network.**

I. Introduction

THE penetration of distributed energy resources (DERs), such as photovoltaic systems, wind turbines, and energy storage devices, has increased over the last few years. DERs are capable of participating in electricity markets [1] and improving resilience of distribution systems [2], [3]. In addition, DERs can provide ancillary services, such as frequency regulation [4] and voltage regulation [5]. However, DERs cannot operate at their maximum export or import capacity at all times due to network limitations [6]. To ensure secure network safety, the concept of dynamic operating envelopes (DOE) is proposed. DOEs specify DERs' power import and export limits at the connection point over a given time interval [7]. By definition, all operating points within these limits comply with operational constraints of the distribution system. In other words, DOEs allow utilities to maintain system security without directly intervening in DER operations and disclosing system topologies.

Building on the above definition, DOE optimization aims at determining the maximal import and export limits at each node. Existing research typically maximizes import and export limits separately based on linear power flow equations, assuming that loads across the distribution system are perfectly forecasted [8]. However, such a method raises several technical concerns. First, feasibility verified only at boundary operating points does not certify that all interior operating points satisfy network constraints [9], [10]. Second, load forecast error is unavoidable. However, existing work typically adopts deterministic formulations that ignore load uncertainty [11], [12]. Third, most linearized power flow models are approximations of the nonconvex alternative current (AC) power flow equations [13], which might incur accuracy concerns in DOE optimization.

Existing studies have attempted to address the feasibility of DOE interior points, but limitations still remain. Some studies have proposed sampling-based methods in which feasible operating points are first identified via power-flow simulations. The DOE is then defined as the convex hull of these points [14], [15], [16]. While this provides a convenient construction, the convex hull may still contain interior points that have never been validated. To strengthen interior feasibility guarantees, other studies verify feasibility at boundary points [17], where feasibility at boundary points is taken to imply feasibility of all convex combinations within the region. However, this method relies on a linearized power-flow model. When more accurate nonlinear network constraints, such as line-current limits, are taken into account, boundary-point feasibility no longer guarantees the feasibility of all interior points. Another approach verifies interior-point feasibility by first constructing an inscribed ellipsoid or superellipsoid within the feasible region and then deriving a hyperbox from it as the DOE [18], [19], [20]. The resulting DOE is conservative because the obtained hyperbox is generally sub-optimal in volume relative to the maximal feasible hyperbox.

Load uncertainty caused by forecasting errors can lead to network-constraint violations even when DERs operate within their allocated DOEs [21]. Therefore, accounting for load uncertainty is essential in DOE optimization if network security is to be guaranteed in practice. Existing uncertainty-aware DOE studies, however, still have important limitations. The piecewise-affine adjustable robust policies are adopted, in which

Received 19 September 2025; revised 15 April 2026; accepted 16 June 2026. This work was supported in part by the U.S. Department of Energy's Office of Critical Minerals and Energy Innovation (CMEI) under the Integrated Energy Systems Office under Award DE- EE0011374 and in part by the National Science Foundation under Grant ECCS 2042314. Paper no. TPWRS-01661-2025. *(Corresponding author: Zhaoyu Wang.)*

The authors are with the Department of Electrical and Computer Engineering, Iowa State University, Ames IA 50011 USA (e-mail: zfx@iastate.edu; hongyili@iastate.edu; wzy@iastate.edu).

Digital Object Identifier 10.1109/TPWRS.2026.3706325

1558-0679 © 2026 IEEE. All rights reserved, including rights for text and data mining, and training of artificial intelligence and similar technologies. Personal use is permitted, but republication/redistribution requires IEEE permission. See https://www.ieee.org/publications/rights/index.html for more information.

IEEE Proof

TABLE I
COMPARISON OF REPRESENTATIVE DOE-RELATED STUDIES AND THE PROPOSED WORK

Reference	Uncertainty handling	Feasibility of all points within DOE	Power flow model		
			ACPF	Physics-based LPF	Data-driven LPF
Ref. [10], [11], [14]–[16], [25], [26], [28]	N/A	×	√	×	×
Ref. [8], [12], [13], [29], [30]	N/A	×	×	√	×
Ref. [31]	N/A	×	×	×	√
Ref. [17]–[20], [27]	N/A	√	×	√	×
Ref. [23]	Piece-wise affine policy	×	√	×	×
Ref. [24]	Robust counterpart	×	×	√	×
Ref. [22]	Piece-wise affine policy	√	√	×	×
This work	Feasibility-based check	√	×	×	√

decision variables are approximated as piecewise-affine functions of uncertainty [22], [23]. Although this formulation improves tractability, the reliance on a prespecified affine structure often leads to conservative DOEs. A robust DOE formulation based on norm-bounded load uncertainty sets is proposed in [24]. However, the resulting DOE is constructed under the additional assumption that all nodes share the same DOE. The resulting DOE can be conservative and does not optimize node-wise DOE bounds while certifying the feasibility of all interior operating points.

In addition to feasibility and uncertainty, the accuracy of DOE optimization is also tied to the power flow model. A central challenge is the trade-off between accuracy and convexity. Several works use full AC power-flow models to accurately capture nonconvex network constraints. DOEs can be obtained either by solving ACOPF with nonlinear solvers [25] or by iteratively tightening DER export limits and validating feasibility via power-flow simulation [26]. These models are accurate but either lack explicit guarantees of global optimality or impose a heavy computational burden. To ease the computational burden, both physics-based [27], [28], [29] and data-driven [30] linearized power flow models have been widely studied. However, such models are not accurate enough. To address this issue, a piecewise-affine convex approximation of the power flow model based on input-convex neural networks (ICNNs) is proposed and applied in DOE optimization in Ref. [31]. Nevertheless, our previous work in Ref. [31] addressed deterministic DOE optimization under nonconvex power-flow constraints by using ICNN-based surrogate models to improve tractability. It doesn't check the robustness of DOE under load uncertainty with feasibility guarantees for all interior operating points within the DOE. This distinction is important because it changes the problem from a single-stage deterministic optimization into a two-stage adaptive robust optimization (ARO) framework, in which the ICNN is used only as a feasibility-check model for robust verification.

Table I summarizes DOE-related studies in the existing literature. The first three groups of studies neither account for load uncertainty nor ensure the feasibility of all interior points in the resulting DOE. The fourth to sixth groups address part of them, while still not addressing both simultaneously. The seventh group of studies further strengthens DOE characterization by considering both aspects using ACPF. Nevertheless, it handles uncertainty through a piecewise-affine policy, which results in a conservative DOE because the recourse decisions are restricted to a prespecified functional of uncertainty. Therefore, although existing studies have addressed parts of the overall problem, a framework that simultaneously accounts for load uncertainty, certifies the feasibility of all points within the DOE, and maintains tractability through an accurate surrogate power-flow model remains lacking. This gap is addressed simultaneously in this paper by proposing a two-stage ARO problem that maximizes the DOE while guaranteeing the feasibility of all interior points under any uncertainty realization.

In summary, most DOE optimization formulations guarantee only boundary point feasibility while neglecting load uncertainty, and the trade-off between power flow model accuracy and computational tractability needs more research. To go over these gaps, first, we propose a DOE optimization framework based on a two-stage ARO problem. The first stage aims to characterize the boundaries of DOE. It is iteratively refined by second-stage feasibility cuts generated from violating interior operating points and uncertainty realizations, which makes it different from many existing DOE algorithms. Consequently, the resulting DOE is guaranteed to be robustly feasible. The second stage checks the robust feasibility, which is defined as the condition that all points inside the DOE under any load uncertainty realization are feasible. An ICNN-based feasibility check model is proposed to ease the computational burdens in the second stage. Moreover, a solution method based on Benders decomposition is leveraged to convert the problem into a mixed integer linear programming problem (MILP). Several case studies are presented, validating the effectiveness of the proposed methods. The contributions of this paper are summarized as follows:

1) A DOE optimization framework is proposed within a two-stage ARO formulation. In each iteration, the first stage optimizes the DOE by maximizing its volume. The second stage verifies robust feasibility for all operating points under all uncertainty realizations. This iterative interaction between the two stages ensures that the final DOE is both maximal in size and guaranteed to be robustly feasible.
2) Based on a data-driven linearized power flow model, a feasibility-check model for DOEs is proposed and integrated into the framework. Compared with the commonly used LinDistFlow-based feasibility-check model in [27],

IEEE Proof

the proposed model preserves linearity while achieving higher robust-feasibility classification accuracy, measured by agreement with OpenDSS.

3) A solution method based on Benders decomposition is proposed. By analyzing the characteristics of uncertainty sets and applying the big-M method, we linearize the bilinear terms and reformulate the DOE optimization into an MILP problem, which is tractable for off-the-shelf solvers.

The remainder of the paper is organized as follows. Section II provides problem formulation, including models of DERs and loads, the AC power flow model, and the DOE optimization problem. Section III presents the ICNN-based feasibility check model, ICNN-based DOE optimization formulation, and the solution method. Section IV reports numerical results that demonstrate the practicality and robustness of the proposed DOE method. Section V concludes with key findings and implications.

II. Problem Formulation

A. Notation

For a distribution system, assume it's a graph $G(V_G, E_G)$ with a vertex set V_G and an edge set E_G. We use $(i,j) \in E_G$ and $i \to j$ to denote an edge that points from node i to node j. $\mathcal{T} := \{1, 2, 3, \ldots, T\}$ is the set of all time intervals, indexed by t. $\mathbf{1}$ represents a vector with all elements equal to 1. I denotes the identity matrix. $\|\cdot\|$ denotes the Euclidean norm.

B. Models of DERs and Loads

In practice, DOE optimization often relies on both DER and load forecasts. This subsection introduces the mathematical models of DERs and uncontrollable loads used in DOE optimization formulation, along with their associated uncertainties.

1) DER Model: The output of DERs is restricted to their power range limits:

$$\underline{p}^{\text{DER}}_{j,t} \le p^{\text{DER}}_{j,t} \le \overline{p}^{\text{DER}}_{j,t}, \tag{1a}$$

$$q^{\text{DER}}_{j,t} = k^{\text{DER}}_{PF} p^{\text{DER}}_{j,t}, \tag{1b}$$

where $p^{\text{DER}}_{j,t}$ and $q^{\text{DER}}_{j,t}$ are the active power and the reactive power injection of DERs at node j at time t, respectively. The output should be limited by its lower bound $\underline{p}^{\text{DER}}_{j,t}$ and upper bound $\overline{p}^{\text{DER}}_{j,t}$. DER can operate under multiple control modes, such as constant reactive power, constant power factor, Volt-Var, Volt-Watt, and Frequency-Watt controls [32]. Among these options, we adopt the constant power factor model. Therefore, we assume without loss of generality that the tangent of the angle corresponding to the power factor k^{DER}_{PF} of nodal power injections is known. In the context of DOE, DER power dispatch happens after the DOEs are optimized, and is uncontrollable by utilities. Thus, in this paper, we consider all possible DER operating points within the optimized DOE and ensure they comply with network constraints under any uncertainty realizations.

2) Load Model: From the utility's perspective, load is uncontrollable, and deviations from load forecasts can impact nodal voltages and branch flows. Hence, load forecast uncertainty is significant for DOE optimization formulations. The nodal active power load is modeled as lying within an interval bounded by its upper and lower forecasts. The uncertainty of uncontrollable load can be formulated as:

$$p^{\text{L}}_{j,t} = \zeta^{\text{L}}_{j,t} \cdot \check{p}^{\text{L}}_{j,t} + (1 - \zeta^{\text{L}}_{j,t}) \cdot \hat{p}^{\text{L}}_{j,t}, \tag{2a}$$

$$q^{\text{L}}_{j,t} = k^{\text{L}}_{PF} \cdot p^{\text{L}}_{j,t}, \tag{2b}$$

$$\mathcal{U} := \left\{ \zeta^{\text{L}} \mid 0 \le \zeta^{\text{L}} \le 1 \right\}, \tag{2c}$$

where $p^{\text{L}}_{j,t}$ is the nodal active power load of node j at time t, which is limited by its upper bound $\hat{p}^{\text{L}}_{j,t}$ and lower bound $\check{p}^{\text{L}}_{j,t}$. Assume the load of all nodes has the same power factor. k^{L}_{PF} is the tangent of the angle corresponding to the power factor. Let the auxiliary variable ζ^{L} represent the uncertainty realization that is from 0 to 1, such that $p^{\text{L}}_{j,t}$ can be any value within this bound. $\mathcal{U}$ is the uncertainty set. In addition, the proposed framework can also be extended to other uncertainty models, such as budgeted uncertainty sets [33]. Such an extension would mainly modify the uncertainty-set definition and the second-stage worst-case reformulation, while the overall two-stage ARO framework would remain unchanged. Therefore, the proposed solution methodology remains directly applicable, and only the uncertainty-set representation and the associated subproblem reformulation need to be adapted.

C. Distribution System Power Flow Model

The AC power flow model provides an accurate description of distribution networks by capturing the relationships among active and reactive power, nodal voltage magnitudes, and branch currents. The AC power flow model based on the branch flow model can be formulated as [34]:

$$p_{ij,t} = \sum_{k:j\to k} p_{jk,t} + p_{j,t} + r_{ij} I_{ij,t}, \quad \forall j \in V_G, \tag{3a}$$

$$q_{ij,t} = \sum_{k:j\to k} q_{jk,t} + q_{j,t} + x_{ij} I_{ij,t}, \quad \forall j \in V_G, \tag{3b}$$

$$p_{j,t} = p^{\text{L}}_{j,t} - p^{\text{DER}}_{j,t}, \quad \forall j \in V_G, \tag{3c}$$

$$q_{j,t} = q^{\text{L}}_{j,t} - q^{\text{DER}}_{j,t}, \quad \forall j \in V_G, \tag{3d}$$

$$V_{j,t} = V_{i,t} - 2r_{ij}p_{ij,t} - 2x_{ij}q_{ij,t} + \left(r^2_{ij} + x^2_{ij}\right) I_{ij,t}, \quad \forall (i,j) \in E_G, \tag{3e}$$

$$I_{ij,t} = \frac{p^2_{ij,t} + q^2_{ij,t}}{V_{i,t}}, \quad \forall (i,j) \in E_G, \tag{3f}$$

$$V_{j,t} \le V^{\max}, \quad V^{\min} \le V_{j,t}, \quad \forall j \in V_G, \tag{3g}$$

$$I_{ij,t} \le I^{\max}_{ij,t}, \quad \forall (i,j) \in E_G, \tag{3h}$$

where $p_{j,t}$ and $q_{j,t}$ denote the net active and reactive power demands at node j and time t, respectively. $p_{ij,t}$ and $q_{ij,t}$ represent the active and reactive power flows from node i to node j at time t. r_{ij} and x_{ij} are the line resistance and reactance. $I_{ij,t}$ is the squared magnitude of the current flowing from node i to node j. $V_{i,t}$ represents the squared voltage magnitudes at nodes i at time t. $V^{\max}$ and $V^{\min}$ are the range of $V_{i,t}$. $I^{\max}_{ij,t}$ is the upper limit of $I_{ij,t}$. Constraints (3a) and (3b) represent

IEEE Proof

the active and reactive power balance constraints; Constraint (3e) defines the voltage drop constraint between node i and node j. Constraint (3f) defines the relationship between branch power flows, squared current magnitude, and squared voltage magnitude. Constraints (3g) and (3h) ensure that the voltage and the current remain within the predefined operating range.

D. DOE Optimization Problem

By definition, DOEs are node-wise power ranges, which are decoupled from each other. Thus, DOEs are typically formulated as a hyperbox, where each controllable variable is limited by its lower and upper bounds. Thus, the DOE can be formulated as $\mathcal{P}$:

$$\mathcal{P} := \{p \mid \underline{p} \le p \le \overline{p}\}, \tag{4}$$

where $\underline{p}$ and $\overline{p}$ are minimum and maximum power limits.

DOE optimization aims to determine the maximum export and maximum import capability of each DER node, while ensuring that every point within the DOE satisfies power flow constraints (3) under any realization of uncertainty. In other words, the DOE optimization problem aims to maximize the feasible region of power injections with the shape defined in (4) and guarantees that, for all possible realizations of load power and for all DER power within the DOE, power flow constraints (3) are not breached. In practice, DOE operation naturally has a here-and-now and wait-and-see structure. The utility first determines the DOE boundaries as operating limits for DERs. After the DOE is issued, DERs may operate at any admissible point within the DOE, while the actual load uncertainty is realized afterward. Therefore, the DOE bounds must be determined before both the DER operating point and the uncertainty realization are known, and feasibility must be guaranteed after they are realized. If neither load uncertainty nor interior-point feasibility is considered, the problem reduces to a deterministic DOE problem, which can be handled in a single-stage formulation. However, in this paper, the requirement is that every operating point within the continuous DOE set must remain feasible under every realization of the continuous uncertainty set. This joint requirement would raise infinitely many feasibility conditions. Therefore, a single-stage formulation is not tractable, which motivates the two-stage ARO formulation.

Accordingly, based on equation (4), the DOE optimization problem can be formulated as an ARO:

$$\min_{\underline{p},\overline{p}} \quad -1^{\top}(\overline{p}-\underline{p}) + \max_{p\in\mathcal{P},\zeta^{\mathrm{L}}\in\mathcal{U}} \min_{y\in Y} \quad 0 \tag{5}$$

where y denotes all variables of the power flow constraints and $Y = \{y \mid f(y,p,\zeta^{\mathrm{L}}) = 0, g(y,p,\zeta^{\mathrm{L}}) \le 0\}$ denotes the feasible region depicted by constraints (1)–(3). Problem (5) follows a two-stage ARO structure. This problem can guarantee that the DOE is *robustly feasible*, which is defined as follows: for every admissible DER operating point $p \in \mathcal{P}$ and every uncertainty realization $\zeta^{\mathrm{L}} \in \mathcal{U}$, there exists a feasible auxiliary variable vector y such that all network and device constraints are satisfied. The outer minimization enlarges the DOE by maximizing its volume. The inner maximin problem checks that for any nodal injection point p together with a load uncertainty realization ζ^{L}, whether there exist feasible operational variables y such that all constraints are satisfied. The minimization of the inner problem is a feasibility check, which tries to find a feasible operating point when given p and ζ^{L}. If a feasible y exists, the objective value of the inner problem equals zero; otherwise, it returns ∞, indicating infeasibility. The maximization of the inner problem examines all possible p and ζ^{L}, and then identifies the worst case. In this way, the optimal DOE obtained by solving problem (5) guarantees that all possible DER power dispatches within the DOE are feasible under any realization of uncertain load power.

Although this paper maximizes DOE size in the first stage, the proposed framework can accommodate different first-stage objectives. Fairness-oriented objectives, such as uniform curtailment [26] or equal curtailment amount [30], can also be incorporated without altering the second-stage robust feasibility verification.

III. Robust DOE Optimization Algorithm

A. ICNN-Based Feasibility Check Model

The second-stage feasibility check in problem (5) requires solving power flow equations under varying DER dispatch and load uncertainties. Due to non-convexity, the AC power flow model can only be applied to specific DER dispatches and load uncertainty realizations. However, it is impossible to enumerate them since both the DOE and the uncertainty set are continuous. In addition, directly embedding ACPF into the second-stage feasibility-check problem would lead to a nonlinear and non-convex formulation, which would need to be solved repeatedly within the iterative robust DOE algorithm. This would reduce tractability and scalability. Conventional convex relaxations, such as SOCP, are also not adopted here because their tightness cannot always be guaranteed for the problem considered [35]. Therefore, a linear surrogate model is preferred for the embedded feasibility check. To do the feasibility check in a more computationally efficient way, we use ICNNs to replace the power flow model in our proposed feasibility check model.

1) Preliminaries of ICNN: Fig. 1 illustrates the architecture of ICNN. The network consists of an input layer, multiple hidden layers, and an output layer. The input variable is denoted by n, while the hidden layer outputs are represented by z_k, and the final output is denoted by m. Each hidden layer is generated through an affine transformation of the input and the previous hidden state, followed by an activation function $\sigma(\cdot)$ [36]. In this paper, we adopt ReLU as the activation function, which leads to a piecewise linear approximation of power flow mappings that can be further relaxed into a linear form. The parameters of the ICNN include the weight matrices W_k^n, W_k^z, and the bias terms b_k, where W_k^z are required to be non-negative to preserve convexity.

2) ICNN-Based Power Flow Model: The forward propagation of an ICNN can be expressed as a sequence of affine transformations and ReLU activations. Specifically, for an input n, the inference of output m can be written as:

$$z_1 = \sigma(W_0^n n + b_0)\,, \tag{6a}$$

$$z_{k+1} = \sigma(W_k^z z_k + W_k^n n + b_k)\,, \quad k = 1,\dots,K-1, \tag{6b}$$

$$m = W_K^z z_K + W_K^n n + b_K. \tag{6c}$$

IEEE Proof

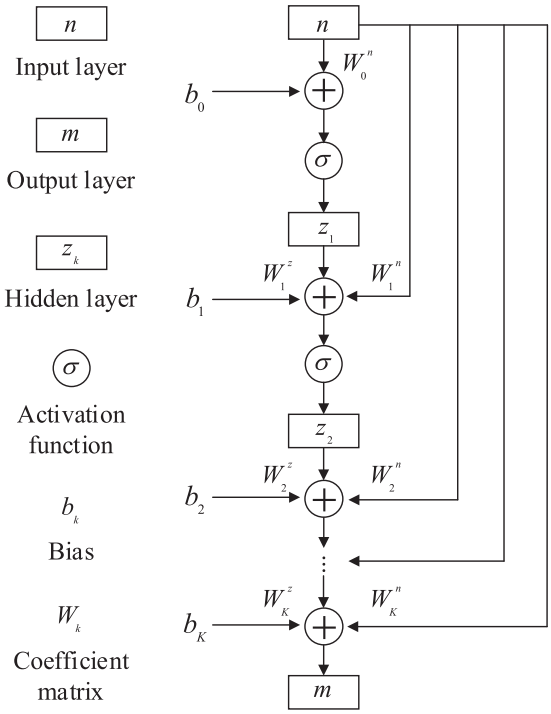

Fig. 1. Diagram of ICNN.

Since $W_k^z \geq 0$ and the activation function ReLU is convex and non-decreasing, the mapping from input n to the output m is guaranteed to be convex.

The ReLU activation $\sigma(u) = \max\{u, 0\}$ can be represented exactly by introducing an auxiliary variable z and the linear inequalities when minimizing the output z:

$$\min_{z} \quad z \tag{7a}$$

$$\text{s.t.} \quad z \geq u, \tag{7b}$$

$$z \geq 0, \tag{7c}$$

where z is the activated output and u is the affine input. When the objective z is minimized, this reformulation provides an exact representation of the ReLU activation.

Thus, the inference of ICNN can be equivalently represented as the minimization of output m subject to a set of linear constraints. Equations (6) are equivalent to:

$$\min_{z_k, m} \quad m \tag{8a}$$

$$\text{s.t.} \quad z_1 \geq W_0^n n + b_0, \quad z_1 \geq 0, \tag{8b}$$

$$z_{k+1} \geq W_k^z z_k + W_k^n n + b_k, \quad z_{k+1} \geq 0,$$

$$k = 1, \ldots, K-1, \tag{8c}$$

$$m \geq W_K^z z_K + W_K^n n + b_K. \tag{8d}$$

The above reformulation makes it possible to embed a trained ICNN as a linear part of optimization models, providing a computationally efficient way to consider power flow constraints, without sacrificing too much accuracy, as we discussed in the following paragraphs.

As discussed in our previous work [31], to preserve convexity, the input of ICNN is the net active and reactive power at all nodes, while the outputs are the nodal voltage magnitudes and line current magnitudes:

$$m^{\text{v}} = \left[V; -V\right], m^{\text{ol}} = I, \tag{9}$$

where V is the bus voltage magnitude vector and I is the line current magnitude vector. We use δ^{v} and δ^{ol} to denote the overall violations of constraints (3g) and (3h):

$$\delta^o = \mathbf{1}^\top \max(m^o + \varepsilon^o, 0), \quad o \in \{\text{v}, \text{ol}\}, \tag{10}$$

where $\varepsilon^{\text{v}} = [-V^{\max}; V^{\min}]$ represents the voltages limits, $\varepsilon^{\text{ol}} = [-I^{\max}]$ represents the line currents limits. δ^o is zero if the corresponding constraints are satisfied and positive otherwise. According to (7), by minimizing $\delta^{\text{v}} + \delta^{\text{ol}}$, equation (10) can be replaced by linear constraints. Thus, the ICNN-based power flow model aims to minimize the violation term subject to the ICNN constraints. Furthermore, by enforcing $\delta^{\text{v}} + \delta^{\text{ol}} = 0$, the formulation becomes a feasibility check model: it determines whether there exist auxiliary variables z_k that drive all violation terms to zero, which is equivalent to verifying that the operating point lies within the feasible region where all constraints are satisfied. Accordingly, we propose an ICNN-based feasibility check model:

$$\min_{z_k^o} \quad 0 \tag{11a}$$

$$\text{s.t.} \quad p_j = p_j^{\text{L}}(\zeta^{\text{L}}) - p_j^{\text{DER}}, \quad \forall j \in V_G, \tag{11b}$$

$$q_j = k_{PF}^L p_j^{\text{L}}(\zeta^{\text{L}}) - k_{PF}^{DER} p_j^{\text{DER}}, \quad \forall j \in V_G, \tag{11c}$$

$$n = \begin{bmatrix} p_j \\ q_j \end{bmatrix}, \tag{11d}$$

$$z_1^o \geq W_0^{n,o} n + b_0^o, \quad z_1^o \geq 0, \quad \forall o \in \{\text{v}, \text{ol}\}, \tag{11e}$$

$$z_{k+1}^o \geq W_k^{z,o} z_k^o + W_k^{n,o} n + b_k^o, \quad z_{k+1}^o \geq 0,$$

$$k = 1, \ldots, K, \quad \forall o \in \{\text{v}, \text{ol}\}, \tag{11f}$$

$$0 \geq W_K^{z,o} z_K^o + W_K^{n,o} n + b_K^o + \varepsilon^o,$$

$$\forall o \in \{\text{v}, \text{ol}\}, \tag{11g}$$

where p_j^{DER} denotes the DER active power injection of node j. The actual net power at each node is denoted by p_j for active power and q_j for reactive power. p_j^{L} is the active loads at node j. $W_0^{n,o}$, $W_k^{z,o}$, $W_k^{n,o}$, b_0^o, and b_k^o are the parameters of ICNN, which are obtained by training the neural network. n denotes the input vector of the ICNN. z_k^o represents the output of the k-th hidden layer. K is the number of hidden layers.

B. ICNN-Based DOE Optimization Formulation

The ICNN-based feasibility-check model derived above provides a tractable surrogate of the power-flow feasibility region, which can then be embedded into the DOE optimization problem. Based on the feasibility check model (11), the ICNN-based

IEEE Proof

ARO problem is:

$$\min_{\underline{p},\overline{p}} \quad -1^\top(\overline{p}-\underline{p}) + \max_{p\in\mathcal{P},\zeta^{\mathrm{L}}\in\mathcal{U}} \quad \min_{y\in Y} \quad 0 \tag{12}$$

where $Y=\{y \mid Ap+B\zeta^{\mathrm{L}}+Cy\le b_0\}$, $y=\{z_k^o \mid k=1,\ldots,K,\ o\in\{\mathrm{v},\mathrm{ol}\}\}$ denotes the collection of all auxiliary variables. The vector $p=\{p_j^{\mathrm{DER}} \mid j\in V_G\}$ denotes nodal active DER power injections, and ζ^{L} captures the uncertain load realizations. Matrices A,B,C and vector b_0 are determined by the trained ICNN parameters W_k and b_k. The proposed ICNN-based feasibility check model relieves the computational burden brought by the power flow model. Comparing to the original problem (5), problem (12) is relatively easier to solve, allowing us to check the feasibility of every point $p\in\mathcal{P}$, together with any uncertainty $\zeta^{\mathrm{L}}\in\mathcal{U}$.

C. Solution Method Based on Benders Decomposition

Although the ICNN-based reformulation makes the feasibility-check problem tractable, the resulting DOE optimization problem still has a two-stage robust structure. To solve problem (12), we further propose a solution method based on Benders' decomposition [33]. The Benders' decomposition reformulates the problem into a master problem and a subproblem, which are solved iteratively to approximate the original two-stage problem. The master problem (first stage) determines and maximizes the DOE. The subproblem (second stage) verifies the feasibility of all operating points within the DOE under the considered uncertainties.

1) Master Problem: According to the Benders decomposition, the master problem is developed as (13). In this optimization, we should make the decision of the first stage with variables $\underline{p},\overline{p}$ to maximize the volume of DOE:

$$\min_{\underline{p},\overline{p}} \quad -\mathbf{1}^\top(\overline{p}-\underline{p}) \tag{13a}$$

$$\text{s.t.} \quad \overline{p}-\underline{p}\ge 0, \tag{13b}$$

$$\mu_l^{*\top}(b_0-Ap_l^{\mathrm{bd}}-B\zeta_l^{\mathrm{L}*})\le 0, \quad l=1,\ldots,N_I, \tag{13c}$$

where μ_l^* and $\zeta_l^{\mathrm{L}*}$ are the solutions of the subproblem under the l–th iteration. p_l^{bd} is corresponding to the sign of $\mu^{*\top}A$. When $\mu^{*\top}A\ge 0$, $p_l^{\mathrm{bd}}=\underline{p}$. When $\mu^{*\top}A\le 0$, $p_l^{\mathrm{bd}}=\overline{p}$. N_I is the total number of iterations. Each iteration adds a feasibility cut to the master problem, changing the feasible region of $\underline{p},\overline{p}$. As more cuts are added, the solution space becomes restricted, eventually converging to a set of bounds that guarantees the optimal value of the subproblem is 0.

2) Subproblem: The subproblem aims to validate whether for any given active power injection $p\in[\underline{p},\overline{p}]$ and load uncertainty $\zeta^L\in\mathcal{U}$, there exists a feasible set of auxiliary variables y such that the constraint violations evaluated by ICNNs are zero. This feasibility check is formulated as:

$$\max_{p\in[\underline{p},\overline{p}],\zeta^{\mathrm{L}}\in\mathcal{U}} \quad \min_{y} \quad 0 \tag{14a}$$

$$\text{s.t.} \quad Ap+B\zeta^{\mathrm{L}}+Cy\le b_0, \tag{14b}$$

The feasibility check described above involves a max–min structure. To obtain a tractable form, one approach is to replace the inner problem by its Lagrangian dual. The strong duality of linear programs guarantees that, when feasible, the primal and dual problems yield identical optimal values. The Lagrangian is given by:

$$\begin{aligned}\mathcal{L}(y,\mu) &= \mu^\top(b_0-Ap-B\zeta^{\mathrm{L}}-Cy)\\ &= \left(-\mu^\top C\right)y+\mu^\top(b_0-Ap-B\zeta^{\mathrm{L}}).\end{aligned} \tag{15}$$

where μ is the dual variable. The Lagrange dual function $\mathcal{G}(\mu)$ is:

$$\mathcal{G}(\mu)=\inf_y \mathcal{L}(y,\mu) \tag{16}$$

Therefore, $\mathcal{G}(\mu)$ equals to $\mu^\top(b_0-Ap-B\zeta^{\mathrm{L}})$ when the conditions that minimize the Lagrangian dual problem meet $\mu^\top C=0$ and $\mu\le 0$; otherwise, $\mathcal{G}(\mu)$ is infinite.

The dual problem of (14) is:

$$\max_{p\in[\underline{p},\overline{p}],\zeta^{\mathrm{L}}\in\mathcal{U},\mu} \quad \mu^\top(b_0-Ap-B\zeta^{\mathrm{L}}) \tag{17a}$$

$$\text{s.t.} \quad 0=\mu^\top C, \quad \mu\le 0. \tag{17b}$$

There are two bilinear terms in equation (17), namely $\mu^\top Ap$ and $\mu^\top B\zeta^{\mathrm{L}}$, which are non-convex. To address this issue, we further reformulate the subproblem according to the properties of the DOE and the uncertainty set. Denote $A=[a_1,a_2,\ldots,a_j,\ldots,a_{NA}]$ and $B=[b_1,b_2,\ldots,b_i,\ldots,b_{NB}]$, then we can rewrite

$$\mu^\top Ap=[\mu^\top a_1\ \ \mu^\top a_2\ \ \cdots\ \ \mu^\top a_j\ \ \cdots]p, \tag{18a}$$

$$\mu^\top B\zeta^{\mathrm{L}}=[\mu^\top b_1\ \ \mu^\top b_2\ \ \cdots\ \ \mu^\top b_i\ \ \cdots]\zeta^{\mathrm{L}}. \tag{18b}$$

For each coefficient $\mu^\top a_j$ and $\mu^\top b_i$, the optimal value of p_j and ζ_i^{L} is determined by its sign: if $\mu^\top a_j\ge 0$, then $p_j=\underline{p}_j$; otherwise, $p_j=\overline{p}_j$. A similar rule applies to ζ_i^{L}. To model this selection in a linear form, binary variables $s_j\in\{0,1\}$ and $s_i\in\{0,1\}$ are introduced, where s_j corresponds to p_j and s_i corresponds to ζ_i^{L}. Using the big-M formulation, the bilinear terms are equivalently linearized as:

$$-(1-s_j)M\le\mu^\top a_j\le s_jM, \tag{19a}$$

$$\mu^\top a_j\underline{p}_j-(1-s_j)M\le w_j^A\le\mu^\top a_j\underline{p}_j+(1-s_j)M, \tag{19b}$$

$$\mu^\top a_j\overline{p}_j-s_jM\le w_j^A\le\mu^\top a_j\overline{p}_j+s_jM, \tag{19c}$$

$$-(1-s_i)M\le\mu^\top b_i\le s_iM, \tag{19d}$$

$$-(1-s_i)M\le w_i^B\le(1-s_i)M, \tag{19e}$$

$$\mu^\top b_i-s_iM\le w_i^B\le\mu^\top b_i+s_iM, \tag{19f}$$

$$s_j,s_i\in\{0,1\}, \tag{19g}$$

where w_j^A and w_i^B are auxiliary variables introduced to represent $\mu^\top a_jp_j$ and $\mu^\top b_i\zeta_i^{\mathrm{L}}$, respectively, and M is a large positive

IEEE Proof

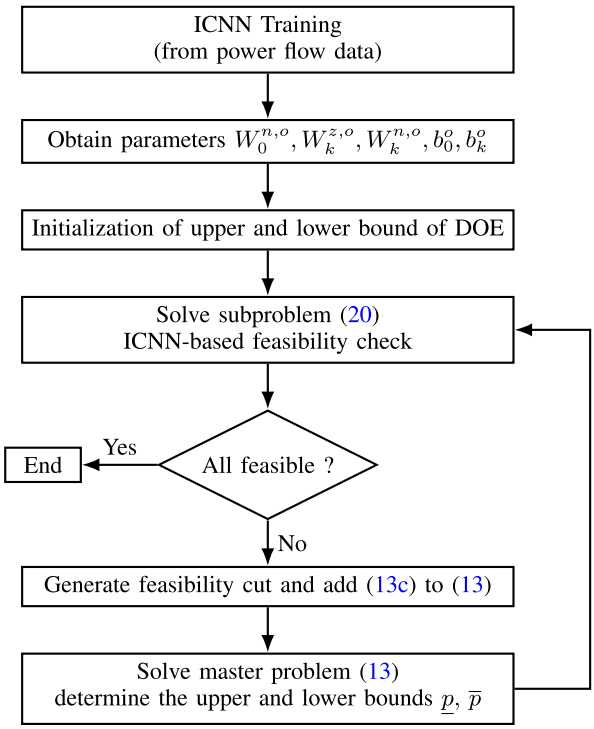

Fig. 2. Flow chart of the proposed DOE optimization method.

constant. The subproblem is reformulated as:

$$\max_{s_i, s_j, \mu, w^A, w^B} \quad \mu^\top b_0 - \sum_j^{NA} w_j^A - \sum_i^{NB} w_i^B \tag{20a}$$

$$\text{s.t.} \quad (17b), \tag{20b}$$

$$(19). \tag{20c}$$

Problem (20) provides a tractable mixed-integer linear reformulation of the intractable subproblem, which can be solved efficiently by off-the-shelf solvers. The worst case of DER power dispatch and load uncertainty realization is captured by the auxiliary variables w_i^A and w_j^B. Assume the optimal solution of (20) is $(\mu^\star, w^{A\star}, w^{B\star}, s_i^\star, s_j^\star)$. When the binary variable $s_i^\star = 0$ and $s_j^\star = 0$, the corresponding component of p or ζ^{L} attains its upper bound, respectively. When $s_i^\star = 1$ and $s_j^\star = 1$, the variable is fixed at its lower bound. By applying this mapping, the realizations $p^\star$ and $\zeta^{\mathrm{L}\star}$ can be obtained.

D. Summary of Proposed DOE Optimization Method

The overall solution procedure is illustrated in Fig. 2, and the iterative Benders decomposition steps are summarized in Algorithm 1. First, an ICNN is trained using historical or simulated power-flow data, from which the weight matrices and bias parameters are extracted. With these parameters fixed, the ICNN is transformed into a linear programming representation of the power-flow constraints and embedded into the proposed two-stage ARO framework. According to the Benders decomposition algorithm, the master problem (13) first determines a candidate DOE by optimizing its lower and upper bounds. For this candidate DOE, the subproblem (20) is then solved to search for a violating operating point inside the DOE together with a load-uncertainty realization. If no violating point is found, i.e., the objective value of the subproblem is smaller than the prescribed tolerance ϵ, then the current DOE is robustly feasible, and the algorithm terminates. Otherwise, the subproblem returns the corresponding violating DOE point, uncertainty realization, and dual variables, which are used to construct a feasibility cut (13c). This cut is then added to the master problem to exclude the current infeasible DOE candidate and tighten the DOE boundaries. After that, the master problem is re-solved to generate a new DOE candidate.

Algorithm 1: Benders Decomposition.

1: Initialize iteration index $l = 1$, tolerance $\epsilon \geq 0$, and DOE bounds $\overline{p}^l$ and $\underline{p}^l$.
2: **while** true **do**
3: Solve subproblem (20) with given $(\overline{p}^l, \underline{p}^l)$ to obtain the optimal solution $(\mu_l^\star, w_l^{A\star}, w_l^{B\star}, s_{i,l}^\star, s_{j,l}^\star)$ and the corresponding $(\zeta_l^{\mathrm{L}\star}, p_l^{\mathrm{bd}})$.
4: **if** the objective value of (20) $\geq \epsilon$ **then**
5: Add the following cut to the master problem (13):

$$\mu_l^{\star\top}\left(b_0 - A p_l^{\mathrm{bd}} - B\zeta_l^{\mathrm{L}\star}\right) \leq 0 \tag{21}$$

6: Update $l \leftarrow l + 1$.
7: Solve master problem (13) to obtain the updated DOE $(\overline{p}^l, \underline{p}^l)$.
8: **else**
9: **break**
10: **end if**
11: **end while**
12: **Output:** the final feasible DOE $(\overline{p}^l, \underline{p}^l)$.

IV. Numerical Study

A. Experiment Setup

In this paper, the IEEE 123-node test feeder and EPRI ckt5 test feeder are used to verify the effectiveness of the proposed approach, shown as Figs. 3 and 4. The nodal voltage magnitudes are constrained to [0.90, 1.10] p.u. on a 4.16-kV base and 7.2-kV base for the IEEE 123-node test feeder and the ckt5 test feeder, respectively. There are 2 three-phase DER buses for the IEEE 123-node test feeder and 4 single-phase DER buses for ckt5 test feeder. Loads of all nodes are assumed to be forecasted. The power factor of both uncontrollable loads and DER outputs is assumed to be 0.95. The optimization problems are solved in MATLAB using Gurobi 12.0. We use OpenDSS to conduct power flow simulations for result validation. For ICNN training, 30,000 samples are generated using OpenDSS. The dataset is split into training, validation, and test sets with a ratio of 64%, 16%, and 20%, respectively. For the IEEE 123-node test feeder, the line current magnitude model uses four hidden layers with 256, 256, 128, and 64 neurons, respectively, while the nodal voltage model uses four hidden layers with 256, 256, 128, and 128 neurons, respectively. For the ckt5 test feeder, the line

IEEE Proof

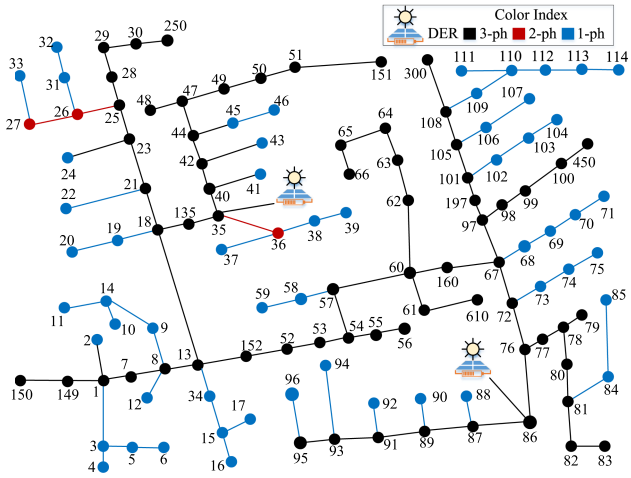

Fig. 3. IEEE 123 bus test system.

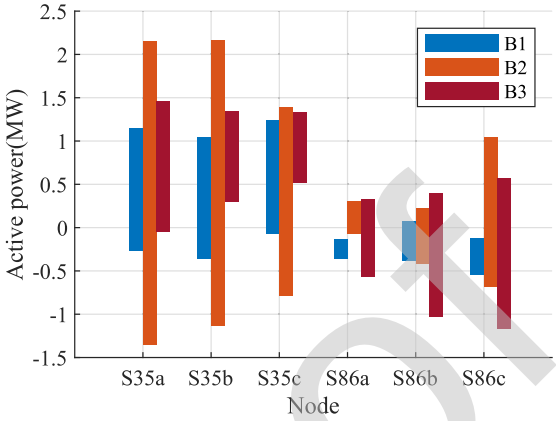

Fig. 5. DOEs of three methods on the IEEE 123-node test feeder.

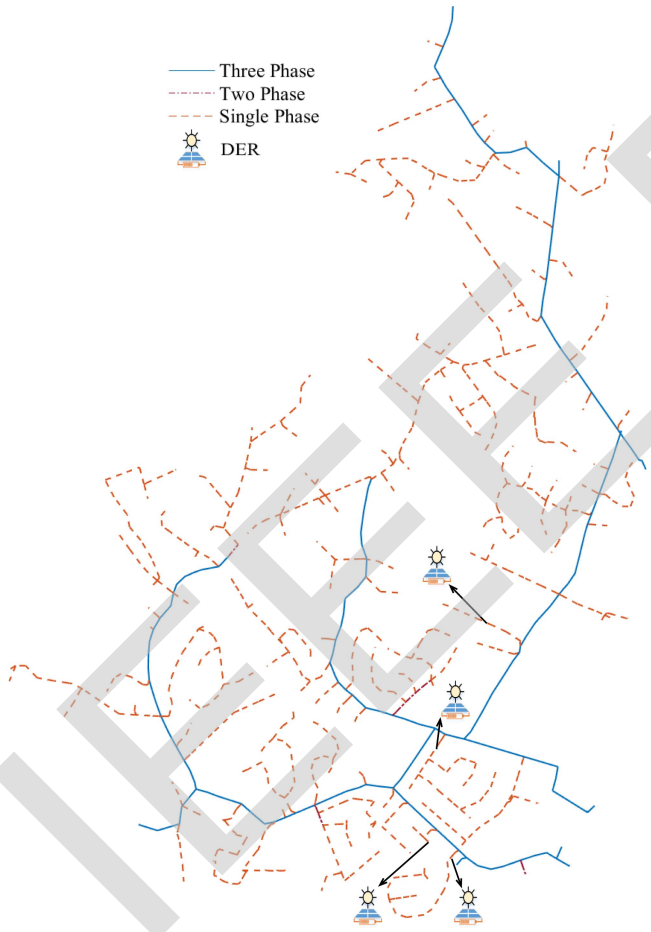

Fig. 4. EPRI ckt5 test system.

current magnitude model uses three hidden layers with 256, 1,028, and 512 neurons, respectively, while the nodal voltage model uses two hidden layers with 512 and 1024 neurons, respectively. Both models are trained using the Adam optimizer with a learning rate of 0.001, a batch size of 200, and 200 epochs. The interval bounds $\check{p}^{\mathrm{L}}$ and $\hat{p}^{\mathrm{L}}$ for uncontrollable nodal loads are synthetically generated from U.S. Midwest utility load data.

To demonstrate the effectiveness of the proposed method, we compare it with the following benchmarks:

1) **B1**: The proposed method, with ICNN-based feasibility check and jointly optimized upper and lower bounds, denoted as ICNN-based DOE (both bounds);
2) **B2**: Joint optimization of DOE upper and lower bounds while using LinDistFlow (LDF) [27] for feasibility check, denoted as LDF-based DOE (both bounds), (see Appendix A for details);
3) **B3**: Optimizing upper/lower bounds of DOE separately with the proposed ICNN-based feasibility check model [31], denoted as ICNN-based DOE (single bound).

B. Validation of DOE Robustness

We first validate whether the final DOE obtained by the proposed method is robustly feasible. The DOE of the proposed method (marked blue) is shown in Fig. 5, which presents the estimated active-power bounds at selected nodes. A pronounced disparity between the upper and lower bounds is observed at node S35, indicating greater flexibility in net injection, whereas nodes S86a–S86c exhibit comparatively narrow bounds. One possible reason is that S35 is closer to the slack bus, while the S86 nodes are near the feeder end, where voltage drop and branch limits tighten the feasible range.

To validate the robustness of the DOE, we employ an optimization-based certification procedure. For a given DER power injection, we verify feasibility under all load uncertainty realizations, as described in detail in Appendix B. 6,000 points within the DOE are randomly sampled and used as the input of the certification problem. Results show that all sampled points are feasible under every uncertainty realization. Therefore, under the ICNN-based feasibility check model, the proposed DOE optimization framework can guarantee the robustness of DOE, i.e., every operating point within the DOE satisfies all network constraints under any uncertainty realization.

C. Impact of Feasibility Check Models

After validating the robustness of the final DOE under the proposed method, we next examine how the feasibility-check

IEEE Proof

TABLE II
COUNTS OF ROBUSTLY FEASIBLE SAMPLES OF ICNN-DOE AND LDF-DOE

	ICNN	LDF	OpenDSS	Samples
Only in ICNN	505	505	501	505
Only in LDF	43	305	59	305
In neither	37	181	44	190

TABLE III
ACCURACY OF ICNN-DOE AND LDF-DOE RELATIVE TO OPENDSS

	ICNN	LDF	OpenDSS
Only in ICNN	99.20%	99.20%	100%
Only in LDF	90.81%	19.34%	100%
In neither	85.78%	26.84%	100%

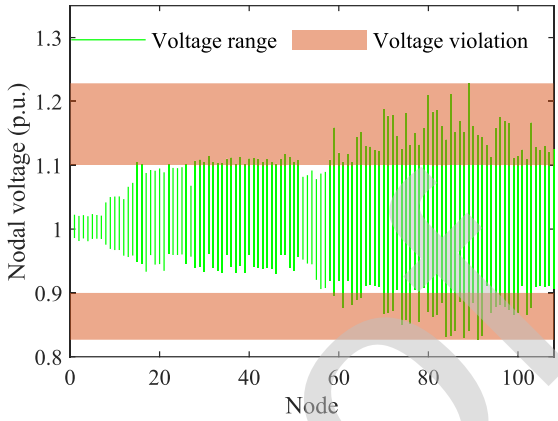

Fig. 6. Nodal voltages distribution for each node when only optimizing a single bound on the IEEE 123-node test feeder.

model affects the resulting DOE characterization. The ICNN-based DOE and LDF-based DOE (marked blue and orange), while jointly optimizing the upper and lower bounds, are shown in Fig. 5. The ICNN-based DOE is generally narrower than the LDF-based DOE. In contrast, the LDF-based DOE remains relatively flat and wider across all nodes, reflecting a less conservative characterization. To compare the accuracy of the ICNN-based and LDF-based DOEs, we randomly sample the power at DER nodes from three disjoint categories: samples only in the ICNN-based DOE, samples only in the LDF-based DOE, and samples in neither DOE. Since OpenDSS cannot directly validate an infinite set of continuous uncertainty realizations, we adopt a sampling-based method to validate robustness [37], [38]. The uncertainty domain [0,1] is discretized into 100 equally spaced uncertainty realizations. For each sample, feasibility is checked against all 100 uncertainty realizations to see if operational constraints are satisfied, using power flow simulation tools like OpenDSS.

In Table II, we report the counts of samples classified as robustly feasible, i.e., feasible for all uncertainty realizations, by the ICNN-based feasibility check model, the LDF-based feasibility check model, and OpenDSS. A sample is labeled 1 if all realizations are satisfied; otherwise, it is labeled 0. Table III summarizes the classification accuracy of the ICNN-based feasibility check model and the LDF-based feasibility check model compared to OpenDSS of each category. Assume the accuracy of OpenDSS is 100%; thus, a higher accuracy means more agreement with OpenDSS.

Table II indicates that the ICNN-based feasibility check model certifies all sampled points of the ICNN-based DOE as feasible under the entire uncertainty set, and the LDF-based feasibility check model analogously certifies the LDF-based DOE. These results confirm the effectiveness of the proposed two-stage ARO-based DOE formulation in guaranteeing robust feasibility. In addition, OpenDSS admits 99.21% samples of the ICNN-based DOE are robustly feasible, while only 20% inner points within the LDF-based DOE are robustly feasible, implying that the seemed less conservative DOE obtained by the LDF model is a result of a less accurate approximation of power flow relationships.

Table III further highlights that in the *Only in ICNN* category, both the ICNN-based and LDF-based feasibility check model achieve a high agreement rate of 99.20% with OpenDSS. In *Only in LDF* and *In neither* categories, however, the ICNN-based feasibility check model maintains a high accuracy of 90.81% and 85.78%, whereas the LDF-based counterpart drops to 19.34% and 26.84%. Overall, the ICNN-based feasibility check model matches OpenDSS better than LDF across all categories and thus serves as a more accurate feasibility oracle.

Thus, the ICNN-based DOE gives a more faithful envelope than its LDF-based counterpart. Consistently, the ICNN-based feasibility check model attains higher agreement with OpenDSS across all categories.

D. Joint Vs. Separate Optimization of DOE Bounds

A widely adopted approach in the literature is to optimize the maximum upper bound or minimum lower bound and verify the feasibility of the bounds. This method does not guarantee that the interior points within the resulting bounds of DOE are feasible under any uncertainty realization. In this section, we compared this conventional method with the proposed joint optimization of upper and lower bounds, with results visualized in Fig. 5 (marked as red and blue). To illustrate the difference, we randomly sampled 1,000 nodal DER power under 100 uncertainty realizations within these two DOEs, respectively. Only 24.2% of *Optimize single bound* category samples satisfy the network constraints across all uncertainty realizations. This indicates that separate optimization of DOE bounds is unreliable for guaranteeing the feasibility of points within the DOE under all uncertainty realizations. Therefore, joint optimization of upper and lower bounds is essential.

Figs. 6 and 7 present the nodal voltage distributions across all samples and uncertainty realizations. When only optimizing a single bound, voltage violations beyond the voltage range of 0.9–1.1 p.u. are observed. This indicates that the conventional single-bound optimization approach fails to adequately constrain voltage magnitudes under uncertainty. By contrast, when both upper and lower bounds are jointly optimized, all nodal voltages remain strictly within the permissible limits for every sample and uncertainty realization.

IEEE Proof

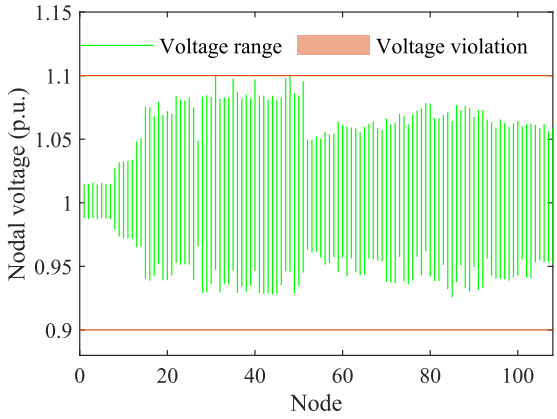

Fig. 7. Nodal voltages distribution for each node when optimizing both bounds on the IEEE 123-node test feeder.

TABLE IV
COMPUTATIONAL TIME OF ICNN AND LDF

Method	Mean time of master problem (s)	Mean time of subproblem (s)	Mean time of total time (s)
ICNN	0.34	1.06	220.37
LDF	0.29	0.39	69.01

E. Time-Series ICNN-Based DOE

We next apply the same iterative workflow to a 24-hour time-series setting to evaluate the computational performance of the proposed method. We use a 24-hour time-series data to optimize the DOE for one operating day. The results are shown in Fig. 8. The robustness of the DOE is validated in the same way as presented in previous subsections. For all buses, the upper and lower bounds of DOE increase from early morning to late afternoon and then decline toward midnight, with the upper limits peaking at approximately 0.5 MW. This pattern is consistent with the total system load profile, which increases through the afternoon and tapers off toward midnight.

To demonstrate computational efficiency, Table IV reports the mean solution time of the master problem, the mean solution time of the subproblem, and the mean total solution time over the 24 time periods for the ICNN-based and LDF-based methods, under a computing environment with an Intel(R) Xeon(R) Gold 5218 CPU (2.30 GHz) and 256 GB RAM. The results show that, although the proposed ICNN-based method requires a longer total solution time than the LDF-based method, the ICNN-based DOE is more accurate than the LDF-based DOE in characterizing the robust feasible region. The ICNN-based feasibility check can screen out more infeasible operating points. This typically leads to more feasibility cuts and, consequently, a larger number of Benders iterations, which explains the longer computational time. Moreover, the mean total solution time of about 220 seconds remains acceptable for practical DOE applications in day-ahead and real-time operational settings, and therefore does not affect the usability of the proposed method.

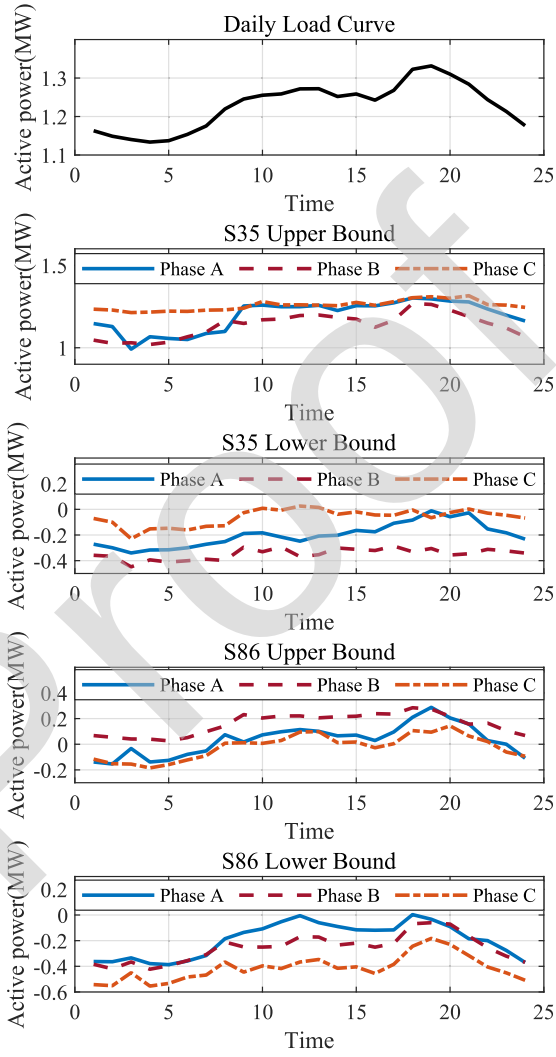

Fig. 8. Daily load curve and time-series ICNN-based DOE on the IEEE 123-node test feeder.

F. Scalability of Proposed Method

To further evaluate the scalability of the proposed method, additional experiments are conducted on the larger EPRI ckt5 feeder. Fig. 9 shows that the three methods produce different DOEs on this larger system. To compare their robust feasibility, 500 operating points are randomly sampled from each DOE, and for each operating point, 100 uncertainty realizations are evaluated. The validation results show that the ICNN-based DOE is more consistent with OpenDSS than the LDF-based DOE. In particular, among the samples lying only in the ICNN-based DOE, OpenDSS confirms 466 out of 500 samples, corresponding to 93.2%, whereas among the samples lying only in the LDF-based DOE, OpenDSS confirms only 312 out of 500 samples, corresponding to 62.4%. In addition, the voltage distributions shown in Figs. 10 and 11 indicate that boundary-point feasibility alone is insufficient, since voltage violations may still occur for interior operating points. These results demonstrate that the proposed framework remains effective on a substantially larger

IEEE Proof

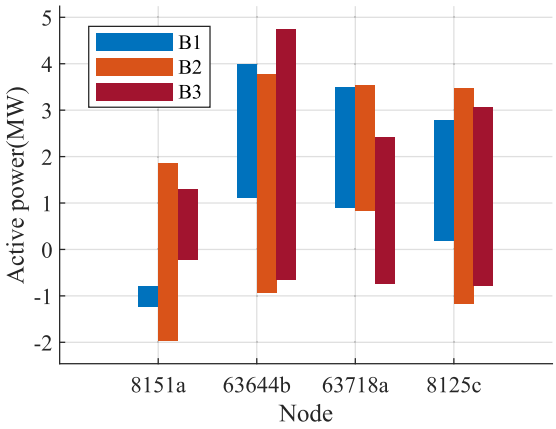

Fig. 9. DOEs of three methods on the ckt5 test feeder.

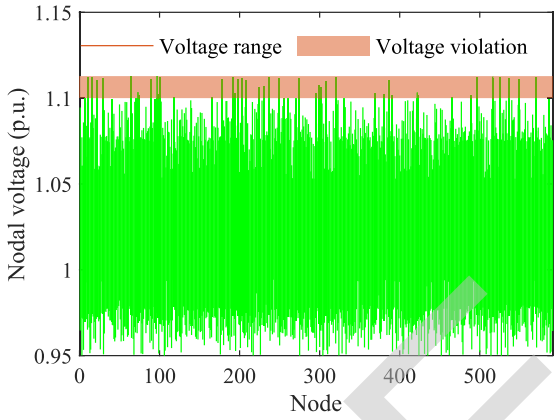

Fig. 10. Nodal voltages distribution for each node when only optimizing a single bound on the ckt5 test feeder.

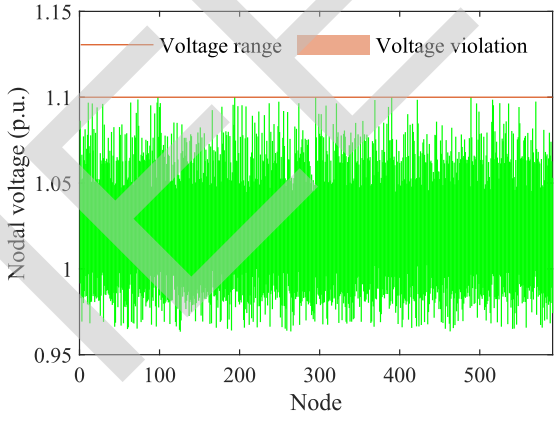

Fig. 11. Nodal voltages distribution for each node when optimizing both bounds on the ckt5 test feeder.

distribution network and that the ICNN-based feasibility-check model provides a more accurate DOE characterization than the LDF-based benchmark.

V. Conclusion

This paper proposes a robust DOE optimization framework that certifies internal feasibility against load uncertainty while retaining computational tractability. We formulate DOE optimization as a two-stage ARO problem: the first stage maximizes the envelope volume, and the second stage verifies the feasibility of all operating points inside the envelope under any realization of uncontrollable loads. To overcome the non-convexity of AC power flow, we embedded an ICNN-based feasibility check model within the ARO. A solution algorithm based on Benders decomposition is further proposed, solving the DOE optimization problem in an iterative manner. Case studies on the IEEE 123-node feeder and EPRI ckt5 test feeder demonstrated that the proposed two-stage ARO-based DOE optimization framework can verify the feasibility of all inner points within the DOE under any uncertainty realization. The ICNN-based DOE achieves a higher classification accuracy of robust feasibility than an LDF-based DOE. We further showed that jointly optimizing upper and lower bounds is critical: separate bound optimization fails to guarantee the feasibility of interior points under uncertainty. The time-series DOEs on a 24-hour horizon were solved within minutes, supporting practical deployment for dynamic updates.

Several directions remain for future work. On the modeling side, the current framework adopts a constant power factor assumption to preserve tractability, whereas practical DERs may also operate under other modes, such as Volt-Var, Watt-Var, constant reactive power, or Volt-Watt control. On the surrogate-modeling side, although the ICNN-based feasibility-check model shows high agreement with OpenDSS, it is still an approximation of the AC power-flow feasibility region. Future work may therefore incorporate uncertainty-quantification tools, such as conformal prediction, to better characterize the surrogate-model prediction error. In addition, although the proposed method is solver-friendly and tractable on the tested system, the size of the coefficient matrices, the number of ICNN auxiliary variables, and the number of binary variables introduced in the reformulated subproblem all will affect solution time on very large feeders.

Appendix A
LDF-Based DOE

The LinDistFlow model can be modeled as:

$$V = V_0 + 2Rp^+ + 2Xq^+, \tag{22a}$$

$$V^{\min} \le V \le V^{\max}, \tag{22b}$$

$$p^+ = -A_1^\top P, \tag{22c}$$

$$|P| \le P^{\max}, \tag{22d}$$

where $p^+ = p^{\text{DER}} - p^{\text{L}}(\zeta^{\text{L}})$ and $q^+ = k_{PF}^{DER} p^{\text{DER}} - k_{PF}^{L} p^{\text{L}}(\zeta^{\text{L}})$ are the net nodal power, p^{DER} and p^{L} are the DER active power injection and the active load power. P denotes the line power. Since line currents are not modeled in LinDistFlow, we approximate the current constraint (3) with a bound on the line active power. V is the squared nodal voltage magnitude. $V^{\min}$, $V^{\max}$, and $P^{\max}$ are the limits of V and P. A_1, R, X,

IEEE Proof

and V_0 are the parameter matrices. According to equation (5), the feasible region of all variables $\tilde{y} = [V; P]$ can be modeled as $\mathcal{P} = \{p \mid \tilde{A}p + \tilde{B}\zeta^{\mathrm{L}} + \tilde{C}\tilde{y} \le \tilde{b}_0, \tilde{D}p + \tilde{E}\zeta^{\mathrm{L}} + \tilde{F}\tilde{y} = \tilde{d}\}$. Similar to the solution method in part C in the Section. III, the LDF-based DOE optimization problem can be decoupled into a master problem and a subproblem. The master problem can be formulated as:

$$\min_{\underline{p},\overline{p}} \quad -\mathbf{1}^\top(\overline{p} - \underline{p}) \tag{23a}$$

$$\text{s.t.} \quad \overline{p} - \underline{p} \ge 0, \tag{23b}$$

$$\gamma_l^{*\top}(\tilde{b}_0 - \tilde{A}p_l^{\mathrm{bd}} - \tilde{B}\zeta_l^{\mathrm{L}*}) + \lambda_l^{*\top}(\tilde{d} - \tilde{D}p_l^{\mathrm{bd}} - \tilde{E}\zeta_l^{\mathrm{L}*}) \le 0, \quad k = 1, \ldots, N_L, \tag{23c}$$

where γ_l^*, λ_l^*, and $\zeta_l^{\mathrm{L}*}$ are the solutions of the subproblem under the l–th iteration. p_l^{bd} is corresponding to the sign of $\gamma_l^{*\top}\tilde{A} + \lambda_l^{*\top}\tilde{B}$. When $\gamma_l^{*\top}\tilde{A} + \lambda_l^{*\top}\tilde{B} \ge 0$, $p_l^{\mathrm{bd}} = \underline{p}$. When $\gamma_l^{*\top}\tilde{A} + \lambda_l^{*\top}\tilde{B} \le 0$, $p_l^{\mathrm{bd}} = \overline{p}$. N_L is the total number of iterations. Each iteration adds a feasibility cut to the master problem.

For the subproblem, the dual subproblem is:

$$\max_{p\in[\underline{p},\overline{p}],\zeta^{\mathrm{L}}\in\mathcal{U},\gamma,\lambda} \quad \gamma^\top(\tilde{b}_0 - \tilde{A}p - \tilde{B}\zeta^{\mathrm{L}}) + \lambda^\top(\tilde{d} - \tilde{D}p - \tilde{E}\zeta^{\mathrm{L}}) \tag{24a}$$

$$\text{s.t.} \quad 0 = \lambda^\top\tilde{F} + \gamma^\top\tilde{C} \tag{24b}$$

$$\gamma \le 0 \tag{24c}$$

where γ and λ are the dual variables.

Assume that:

$$\tilde{A} = [\tilde{a}_1,\ \tilde{a}_2,\ \cdots\ \tilde{a}_j,\ \cdots, \tilde{a}_{N\tilde{A}}], \tag{25a}$$

$$\tilde{B} = [\tilde{b}_1,\ \tilde{b}_2,\ \cdots\ \tilde{b}_i,\ \cdots, \tilde{b}_{N\tilde{B}}], \tag{25b}$$

$$\tilde{D} = [\tilde{d}_1,\ \tilde{d}_2,\ \cdots\ \tilde{d}_j,\ \cdots, \tilde{d}_{N\tilde{A}}], \tag{25c}$$

$$\tilde{E} = [\tilde{e}_1,\ \tilde{e}_2,\ \cdots\ \tilde{e}_i,\ \cdots, \tilde{e}_{N\tilde{B}}], \tag{25d}$$

The dual subproblem is reformulated as:

$$\max_{\tilde{s}_i,\tilde{s}_j,\gamma,\lambda,\tilde{w}^A,\tilde{w}^B} \quad \gamma^\top\tilde{b}_0 - \sum_j^{N\tilde{A}} w_j^A - \sum_i^{N\tilde{B}} w_i^B + \lambda^\top\tilde{d} \tag{26a}$$

$$\text{s.t.} \quad 0 = \lambda^\top\tilde{F} + \gamma^\top\tilde{C} \tag{26b}$$

$$\gamma \le 0 \tag{26c}$$

$$\tilde{s}_j M_L \ge \gamma^\top\tilde{a}_j + \lambda^\top\tilde{d}_j \ge -(1-\tilde{s}_j)M_L \tag{26d}$$

$$(\gamma^\top\tilde{a}_j + \lambda^\top\tilde{d}_j)\underline{p}_j + (1-\tilde{s}_j)M_L \ge w_j^A \ge (\gamma^\top\tilde{a}_j + \lambda^\top\tilde{d}_j)\underline{p}_j - (1-\tilde{s}_j)M_L \tag{26e}$$

$$(\gamma^\top\tilde{a}_j + \lambda^\top\tilde{d}_j)\overline{p}_j + \tilde{s}_j M_L \ge w_j^A \ge (\gamma^\top\tilde{a}_j + \lambda^\top\tilde{d}_j)\overline{p}_j - \tilde{s}_j M_L \tag{26f}$$

$$\tilde{s}_i M_L \ge \gamma^\top\tilde{b}_i + \lambda^\top\tilde{e}_i \ge -(1-\tilde{s}_i)M_L \tag{26g}$$

$$(1-\tilde{s}_i)M_L \ge w_i^B \ge -(1-\tilde{s}_i)M_L \tag{26h}$$

$$(\gamma^\top\tilde{b}_i + \lambda^\top\tilde{e}_i) + \tilde{s}_i M_L \ge w_i^B \ge (\gamma^\top\tilde{b}_i + \lambda^\top\tilde{e}_i) - \tilde{s}_i M_L \tag{26i}$$

$$\tilde{s}_j, \tilde{s}_i \in \{0, 1\} \tag{26j}$$

where w_j^A and w_i^B are auxiliary variables introduced to represent $\gamma^\top\tilde{a}_j p_j + \lambda^\top\tilde{d}_j p_j$ and $\gamma^\top\tilde{b}_i\zeta_i^{\mathrm{L}} + \lambda^\top\tilde{e}_i\zeta_i^{\mathrm{L}}$, respectively, and M_L is a sufficiently large positive constant.

Appendix B
Validation Method

Given any power injection of DER p, we want to verify that for any uncertainty realization, there will be nodal voltages and power flow that don't violate any network constraints. Based on equation (5), this can be formulate as:

$$\max_{\zeta^{\mathrm{L}}\in\mathcal{U}} \ \min_{y\in Y} 0 \tag{27}$$

where y denotes all variables, $Y = \{y \mid Ap + B\zeta^{\mathrm{L}} + Cy \le b_0\}$ denotes all inequality and equality constraints. Similar to the solution method in part C in the Section III, the Lagrangian dual formulation and reformulation are given below. The dual subproblem is:

$$\max_{\zeta^{\mathrm{L}}\in\mathcal{U},\mu} \quad \mu^\top(b_0 - Ap - B\zeta^{\mathrm{L}}) \tag{28a}$$

$$\text{s.t.} \quad 0 = \mu^\top C \tag{28b}$$

$$\mu \le 0 \tag{28c}$$

where μ is the dual variable.

The dual subproblem is reformulated as:

$$\max_{s_i,\mu,w^B} \quad \mu^\top(b_0 - Ap) - \sum_i^{NB} w_i^B \tag{29a}$$

$$\text{s.t.} \quad 0 = \mu^\top C \tag{29b}$$

$$\mu \le 0 \tag{29c}$$

$$s_i M \ge \mu^\top b_i \ge -(1-s_i)M \tag{29d}$$

$$(1-s_i)M \ge w_i^B \ge -(1-s_i)M \tag{29e}$$

$$\mu^\top b_i + s_i M \ge w_i^B \ge \mu^\top b_i - s_i M \tag{29f}$$

$$s_i \in \{0, 1\} \tag{29g}$$

where w_i^B is auxiliary variables introduced to represent $\mu^\top b_i\zeta_i^{\mathrm{L}}$, and M is a sufficiently large positive constant. NB is the number of columns in B.

Therefore, if the reformulated subproblem is 0, we can say that given a power sample, for any uncertainty realization, there will be no constraint violation.

References

[1] Z. Wang, B. Chen, J. Wang, M. M. Begovic, and C. Chen, "Coordinated energy management of networked microgrids in distribution systems," *IEEE Trans. Smart Grid*, vol. 6, no. 1, pp. 45–53, Jan. 2015.

IEEE Proof

[2] Z. Wang and J. Wang, "Self-healing resilient distribution systems based on sectionalization into microgrids," *IEEE Trans. Power Syst.*, vol. 30, no. 6, pp. 3139–3149, Nov. 2015.
[3] Z. Wang, B. Chen, J. Wang, and C. Chen, "Networked microgrids for self-healing power systems," *IEEE Trans. Smart Grid*, vol. 7, no. 1, pp. 310–319, Jan. 2016.
[4] T. Anderson et al., "Frequency regulation with heterogeneous energy resources: A realization using distributed control," *IEEE Trans. Smart Grid*, vol. 12, no. 5, pp. 4126–4136, Sep. 2021.
[5] I. Murzakhanov, S. Gupta, S. Chatzivasileiadis, and V. Kekatos, "Optimal design of volt/VAR control rules for inverter-interfaced distributed energy resources," *IEEE Trans. Smart Grid*, vol. 15, no. 1, pp. 312–323, Jan. 2024.
[6] Y. Huang and L. Söder, "An investigation on the impacts of distributed generation curtailment regulations on distribution network investment," *Elect. Power Syst. Res.*, vol. 145, pp. 175–184, 2017.
[7] "On the calculation and use of dynamic operating envelopes," Australian Renewable Energy Agency, Tech. Rep., Mar. 2021. [Online]. Available: https://arena.gov.au/assets/2020/09/on-the-calculation-and-use-of-dynamic-operating-envelopes.pdf
[8] M. Z. Liu, L. F. Ochoa, P. K. C. Wong, and J. Theunissen, "Using OPF-based operating envelopes to facilitate residential DER services," *IEEE Trans. Smart Grid*, vol. 13, no. 6, pp. 4494–4504, Jun. 2022.
[9] K. Petrou et al., "Ensuring distribution network integrity using dynamic operating limits for prosumers," *IEEE Trans. Smart Grid*, vol. 12, no. 5, pp. 3877–3888, Sep. 2021.
[10] M. M. Hoque, M. Khorasany, M. I. Azim, R. Razzaghi, and M. Jalili, "A framework for prosumer-centric peer-to-peer energy trading using network-secure export–import limits," *Appl. Energy*, vol. 361, 2024, Art. no. 122906.
[11] A. Wickramasinghe, M. Vilathgamuwa, G. Nourbakhsh, and P. Corry, "A multi-objective framework for EV scheduling: Balancing profit and longevity under dynamic operating envelopes," in *Proc. IEEE Ind. Appl. Soc. Annu. Meeting*, 2025, pp. 1–8.
[12] Y. Z. Gerdroodbari, M. Khorasany, and R. Razzaghi, "Dynamic PQ operating envelopes for prosumers in distribution networks," *Appl. Energy*, vol. 325, 2022, Art. no. 119757.
[13] M. R. Alam, P. T. H. Nguyen, L. Naranpanawe, T. K. Saha, and G. Lankeshwara, "Allocation of dynamic operating envelopes in distribution networks: Technical and equitable perspectives," *IEEE Trans. Sustain. Energy*, vol. 15, no. 1, pp. 173–186, Jan. 2024.
[14] G. Lankeshwara, R. Sharma, M. Alam, R. Yan, and T. K. Saha, "Development and validation of a dynamic operating envelopes-enabled demand response scheme in low-voltage distribution networks," *Appl. Energy*, vol. 382, 2025, Art. no. 125150.
[15] G. Lankeshwara and R. Sharma, "Dynamic operating envelopes-enabled demand response in low-voltage residential networks," in *Proc. IEEE PES 14th Asia-Pacific Power Energy Eng. Conf.*, 2022, pp. 1–7.
[16] G. Lankeshwara, R. Sharma, R. Yan, T. K. Saha, and J. V. Milanović, "Time-varying operating regions of end-users and feeders in low-voltage distribution networks," *IEEE Trans. Power Syst.*, vol. 39, no. 2, pp. 4600–4611, Feb. 2024.
[17] J. S. Russell, P. Scott, and J. Iria, "Robust operating envelopes with phase unbalance constraints in unbalanced three-phase networks," in *Proc. IEEE PES Innov. Smart Grid Technol. - Asia*, 2023, pp. 1–5.
[18] B. Liu and J. H. Braslavsky, "Robust dynamic operating envelopes for DER integration in unbalanced distribution networks," *IEEE Trans. Power Syst.*, vol. 39, no. 2, pp. 3921–3936, Mar. 2024.
[19] B. Liu and J. H. Braslavsky, "Computation of robust dynamic operating envelopes based on non-convex OPF for unbalanced distribution networks," *CSEE J. Power Energy Syst.*, early access, Sep. 19, 2024, doi: 10.17775/CSEEJPES.2024.03220.
[20] B. Liu and J. H. Braslavsky, "Robust dynamic operating envelopes via superellipsoid-based convex optimisation in unbalanced distribution networks," *IEEE Trans. Power Syst.*, vol. 39, no. 2, pp. 4775–4778, Mar. 2024.
[21] B. Liu and J. H. Braslavsky, "Sensitivity and robustness issues of operating envelopes in unbalanced distribution networks," *IEEE Access*, vol. 10, pp. 92789–92798, 2022.
[22] A. Attarha, S. Mahdi Noori, R. A. P. Scott, and S. Thiébaux, "Network-secure envelopes enabling reliable DER bidding in energy and reserve markets," *IEEE Trans. Smart Grid*, vol. 13, no. 3, pp. 2050–2062, May 2022.
[23] A. Attarha, M. Mahmoodi, S. M. N. R. A., P. Scott, J. Iria, and S. Thiébaux, "Adjustable price-sensitive DER bidding within network envelopes," *IEEE Trans. Energy Markets, Policy Regulation*, vol. 1, no. 4, pp. 248–258, Dec. 2023.
[24] B. Liu, J. H. Braslavsky, and N. Mahdavi, "Linear OPF-based robust dynamic operating envelopes with uncertainties in unbalanced distribution networks," *J. Modern Power Syst. Clean Energy*, vol. 12, no. 4, pp. 1320–1326, 2024.
[25] M. I. Azim et al., "Dynamic operating envelope-enabled P2P trading to maximize financial returns of prosumers," *IEEE Trans. Smart Grid*, vol. 15, no. 2, pp. 1978–1990, Mar. 2024.
[26] M. I. Azim, M. M. Hoque, M. Khorasany, R. Razzaghi, M. Jalili, and D. J. Hill, "Dynamic operating envelope-integrated cooperative energy trading: A fair allocation approach," *IEEE Trans. Power Syst.*, vol. 40, no. 4, pp. 2845–2859, Jul. 2025.
[27] J. S. Russell, P. Scott, and J. Iria, "Network-secure aggregator operating regions with flexible dispatch envelopes in unbalanced systems," *Elect. Power Syst. Res.*, vol. 235, 2024, Art. no. 110728.
[28] K. Petrou, M. Z. Liu, A. T. Procopiou, L. F. Ochoa, J. Theunissen, and J. Harding, "Operating envelopes for prosumers in lv networks: A weighted proportional fairness approach," in *Proc. IEEE PES Innov. Smart Grid Technol. Eur.*, 2020, pp. 579–583.
[29] M. M. Hoque, M. Khorasany, M. I. Azim, R. Razzaghi, and M. Jalili, "Dynamic operating envelope-based local energy market for prosumers with electric vehicles," *IEEE Trans. Smart Grid*, vol. 15, no. 2, pp. 1712–1724, Mar. 2024.
[30] A. Kumarawadu, M. I. Azim, M. Khorasany, R. Razzaghi, and R. Heidari, "Smart meter data-driven dynamic operating envelopes for DERs," *Appl. Energy*, vol. 384, 2025, Art. no. 125469.
[31] H. Li, L. Liu, Y. Li, and Z. Wang, "Exploiting convexity of neural networks in dynamic operating envelope optimization for distributed energy resources," 2025. Q4
[32] IEEE Standard for Interconnection and Interoperability of Distributed Energy Resources with Associated Electric Power Systems Interfaces, IEEE Standard 1547-2018, Apr. 2018. Q5
[33] D. Bertsimas, E. Litvinov, X. A. Sun, J. Zhao, and T. Zheng, "Adaptive robust optimization for the security constrained unit commitment problem," *IEEE Trans. Power Syst.*, vol. 28, no. 1, pp. 52–63, Jan. 2013. Q6
[34] M. Baran and F. Wu, "Optimal capacitor placement on radial distribution systems," *IEEE Trans. Power Del.*, vol. 4, no. 1, pp. 725–734, Jan. 1989.
[35] H. Moring and J. L. Mathieu, "Inexactness of second order cone relaxations for calculating operating envelopes," in *Proc. IEEE Int. Conf. Commun., Control, Comput. Technol. Smart Grids*, 2023, pp. 1–6.
[36] B. Amos, L. Xu, and J. Z. Kolter, "Input convex neural networks," in *Proc. 34th Int. Conf. Mach. Learn.*, vol. 70, 2017, pp. 146–155.
[37] X. Chen, E. Dall'Anese, C. Zhao, and N. Li, "Aggregate power flexibility in unbalanced distribution systems," *IEEE Trans. Smart Grid*, vol. 11, no. 1, pp. 258–269, Jan. 2020.
[38] X. Chen and N. Li, "Leveraging two-stage adaptive robust optimization for power flexibility aggregation," *IEEE Trans. Smart Grid*, vol. 12, no. 5, pp. 3954–3965, Sep. 2021.

Feixiang Zhang received the B.S. degree in electrical engineering and automation from Anhui University, Hefei, China, in 2019, and the M.S. degree in electrical engineering from the Shanghai University of Electric Power, Shanghai, China, in 2023. He is currently working toward the Ph.D. degree in electrical engineering with Iowa State University, Ames, IA, USA. His research interests include aggregate flexibility and dynamic operating envelopes for distributed energy resources.

IEEE Proof

Hongyi Li (Member, IEEE) received the B.Eng. degree from the Huazhong University of Science and Technology, Wuhan, China, in 2020, the M.Sc. degree from Imperial College London, London, U.K., in 2021, and the Ph.D. degree from the University of Macau, China, in 2024. From 2024 to 2026, he was a Postdoctoral Researcher with Iowa State University. He is currently a Research Engineer with China Southern Power Grid, China. His research interests include AI-aided optimization, power sector decarbonization, distributed energy resource operation, and other smart energy technologies.

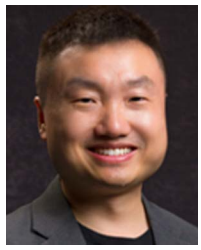

Zhaoyu Wang (Fellow, IEEE) received the B.S. and M.S. degrees in electrical engineering from Shanghai Jiao Tong University, Shanghai, China, and the M.S. and Ph.D. degrees in electrical and computer engineering from the Georgia Institute of Technology, Atlanta, GA, USA. Since 2015, he has been Assistant, Associate, and Full Professor with Iowa State University. His research interests include optimization and data analytics in power distribution systems and microgrids. He was the recipient of the National Science Foundation CAREER Award, IEEE Power and Energy Society (PES) Outstanding Young Engineer Award, ISU Award for Mid-Career Achievement in Research, Northrop Grumman Endowment, ISU College of Engineering's Early Achievement in Research Award, and Harpole-Pentair Young Faculty Award Endowment. He is also the lead Principal Investigator for more than $24 M projects funded by the National Science Foundation, Department of Energy, National Laboratories, PSERC, and Iowa Economic Development Authority. He is the Vice Chair of IEEE Power System Operation, Planning and Economics (PSOPE) Committee, Chair of IEEE Distribution System Operation and Planning Subcommittee, Secretary of IEEE Task Force on IEEE P3102 Standard for Conservation Voltage Reduction (CVR) Data Collection and Management Procedures, and Chair of IEEE Task Force on Advances in Natural Disaster Mitigation Methods. He is also a fellow of IET, and an IEEE PES Distinguished Lecturer.

IEEE Proof